

A method for the forward modelling of 3D electromagnetic quasi-static problems

D.A. Aruliah* U. M. Ascher[†] E. Haber[‡]
D. Oldenburg[§]

August 15, 1999

Abstract

We present a solution method for solving electromagnetic problems in three dimensions in parameter regimes where the quasi-static approximation applies and the permeability is constant. Firstly, by using a potential formulation with a Coulomb gauge, we circumvent the ill-posed problem in regions of vanishing conductivity, obtaining an elliptic, weakly coupled system of differential equations. The system thus derived is strongly elliptic, which leads to reliable discretizations. Secondly, we derive a robust finite-volume discretization. Thirdly, we solve the resulting large, sparse algebraic systems using preconditioned Krylov-space methods. A particularly efficient algorithm results from the combination of BICGSTAB and a block preconditioner using an incomplete LU-decomposition of the dominant system blocks only. We demonstrate the efficacy of our method in several numerical experiments.

Keywords: vector potential, Coulomb gauge, Maxwell's equations, finite volume, Krylov methods, preconditioning.

*Department of Computer Science, University of British Columbia, Vancouver, BC, V6T 1Z4, Canada. (dhavide@cs.ubc.ca).

[†]Department of Computer Science and Institute of Applied Mathematics, University of British Columbia, Vancouver, BC, V6T 1Z4, Canada. (ascher@cs.ubc.ca).

[‡]Department of Computer Science and Institute of Applied Mathematics, University of British Columbia, Vancouver, BC, V6T 1Z4, Canada. (haber@cs.ubc.ca).

[§]Department of Earth and Ocean Science, University of British Columbia, Vancouver, BC, V6T 1Z4, Canada. (doug@geop.ubc.ca).

1 Introduction

We consider Maxwell's equations in the frequency domain. The equations are defined over a domain involving both ground and air [17, 8, 16]. This particular model is used in geophysical surveys where artificial or natural sources induce currents in conducting bodies. A specific example is a magnetotelluric experiment [26] where electric and magnetic fields induced by the sun are measured at the surface of the earth. A major obstacle in modelling such phenomena is that the conductivity in the air essentially vanishes. From an analytic perspective, the specific subset of Maxwell's equations typically used forms a singular system in regions of vanishing conductivity. Even in the ground, where the conductivity is strictly positive, the resulting differential operator is not strongly elliptic. Finding effective methods for solving the linear algebraic systems arising from careful, conservative discretizations such as the ones described in [17, 14, 21] has proved elusive in practice. Such methods are of particular importance in recovering the conductivity profile from measurements of the electric and magnetic fields. In such inverse problems, solving the forward modelling problem presented here is the major bottleneck [22].

We present robust, efficient methods for the simulation of this forward modelling problem. Our development involves three stages. Firstly, we use a Helmholtz decomposition with a Coulomb gauge to obtain a strongly elliptic, weakly coupled system of differential equations. Secondly, we derive a robust finite-volume discretization for these differential equations. Thirdly, we solve the resulting large, sparse algebraic systems using preconditioned Krylov space methods [18, 1]. Combining BICGSTAB and a preconditioner comprising an incomplete LU-decomposition of the dominant system blocks results in a particularly efficient algorithm. We demonstrate the efficacy of our method in several numerical experiments.

The paper is organized as follows. In Section 2, we review Maxwell's equations in the frequency domain. Using the quasi-static assumption and secondary fields, we derive a formulation more suitable for numerical purposes. Our alternative formulation involves a Helmholtz decomposition, splitting the electric field into components in the active space and in the null space of the **curl** operator. This decomposition, used also in [3, 8, 15], leads to a strongly elliptic system. We isolate the singular part of the problem and suggest a strategy for dealing with it using the full system of Maxwell's equations. The result of this formulation is a system that is analogous to a system

in computational fluid dynamics; this analogy to prior work [19] motivates our numerical study.

In Section 3, we construct a straightforward discrete model of the electromagnetic problem from Section 2. The continuous problem is discretized using a finite-volume approach on a simple grid. This discretization avoids the difficulties of finite elements [3, 8, 2] or staggered grids [5, 9, 13], and works well so long as local variations in the conductivity are not too extreme. The discretization reduces the analytic problem to a complex, sparse, block-diagonally dominant system of linear equations.

In Section 4, we discuss the application of Krylov space methods to solve the system of linear algebraic equations. We construct a powerful preconditioner that exploits the block-diagonal dominance of the linear system. The fact that the linear system is block-diagonally dominant is a direct consequence of the fact that the derived continuous formulation is a weakly-decoupled, strongly-elliptic system of partial differential equations (PDEs).

Finally, we present the results of numerical experiments in Section 5. Trials with a synthetic problem verify the second-order accuracy of the discretization. Using various preconditioners and Krylov space methods, we identify a robust solver of the discretized problem. We demonstrate the efficacy of this solver and we show the strength of our formulation (ie. using the Helmholtz decomposition) over the standard formulation of the forward modelling problem (which uses electric fields only) as presented in [17, 20, 21]. We end with the results of our method when used to model a physically-realistic magnetotelluric (MT) experiment.

2 The Electromagnetic Problem

Maxwell's equations in frequency domain read

$$\nabla \times \mathbf{E} - i\omega\mu\mathbf{H} = \mathbf{J}_m, \quad (2.1a)$$

$$\nabla \times \mathbf{H} - (\sigma - i\omega\epsilon)\mathbf{E} = \mathbf{J}_e, \quad (2.1b)$$

$$\nabla \cdot \mathbf{H} = 0. \quad (2.1c)$$

In (2.1), \mathbf{E} is the electric field, \mathbf{H} is the magnetic field, and \mathbf{J}_m and \mathbf{J}_e are magnetic and electric source currents respectively. The permittivity ϵ and the permeability μ are assumed to be constants; in particular, $\epsilon = 8.85 \times 10^{-12}$ F/m and $\mu = 4\pi \times 10^{-7}$ H/m. The conductivity σ is assumed to be piecewise

constant with $\sigma > 0$ in the ground and $\sigma \equiv 0$ in the air. The frequency ω is a known constant as well. The free charge density ρ_f satisfies the relation

$$\nabla \cdot \mathbf{E} = \frac{\rho_f}{\epsilon}. \quad (2.2)$$

Generally, ρ_f is an unknown scalar field, so (2.2) usually defines it.

These partial differential equations (PDEs) are defined in a 3D spatial domain Ω and are subject to Dirichlet boundary conditions of the form

$$\mathbf{E}(x, y, z)|_{\partial\Omega} = \mathbf{g}_1(x, y, z)|_{\partial\Omega} \quad \text{and} \quad (2.3a)$$

$$\mathbf{H}(x, y, z)|_{\partial\Omega} = \mathbf{g}_2(x, y, z)|_{\partial\Omega}, \quad (2.3b)$$

where \mathbf{g}_1 and \mathbf{g}_2 are known vector-valued functions, and $\partial\Omega$ denotes the outer boundary of Ω . The forward modelling problem involves solving the system of PDEs (2.1) with boundary conditions (2.3) for the unknown fields \mathbf{E} and \mathbf{H} , assuming the conductivity σ is known.

In many geophysical applications, the domain Ω is composed of disjoint parts Ω_1 , Ω_2 , and Γ , with $\Omega = \Omega_1 \cup \Omega_2 \cup \Gamma$ (see Figure 1). Physically, Ω_1 is the ground, Ω_2 is the air, and Γ is the interface between the air and ground. Moreover, the domain Ω is unbounded in principle (ie. $\Omega = \mathbb{R}^3$), but, in practice, a bounded, convex subdomain of \mathbb{R}^3 is used for numerical approximations.

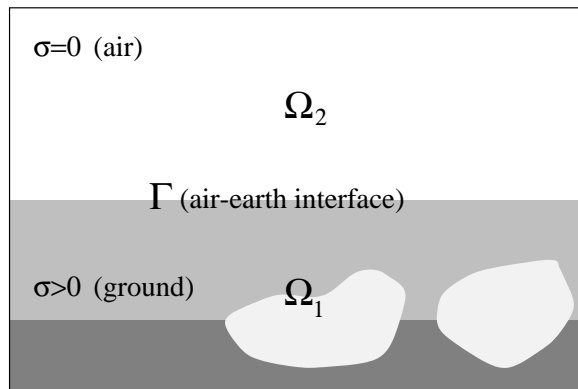


Figure 1: Spatial domain for the forward modelling problem. The conductivity σ is piecewise constant in Ω_1 , distinct regions corresponding to distinct types of matter.

2.1 The quasi-static approximation

Before solving Maxwell's equations (2.1), we make an assumption often referred to as the quasi-static approximation, namely, that the displacement current term $\iota\omega\epsilon\mathbf{E}$ in (2.1b) is very small relative to the other terms. As shown in [23], this assumption holds for most geophysical applications with frequencies ranging from 10^{-3} to 10^6 Hz. Thus, the system we study is

$$\nabla \times \mathbf{E} - \iota\omega\mu\mathbf{H} = \mathbf{J}_m, \quad (2.4a)$$

$$\nabla \times \mathbf{H} - \sigma\mathbf{E} = \mathbf{J}_e, \quad (2.4b)$$

$$\nabla \cdot \mathbf{H} = 0 \quad (2.4c)$$

together with (2.3) and (2.2).

2.2 Secondary fields

In many cases in geophysics, the electric and magnetic source currents \mathbf{J}_e and \mathbf{J}_m are highly localized. As such, we can encounter numerical difficulties caused by large values of the fields \mathbf{E} and \mathbf{H} close to the sources. It is convenient to reformulate (2.4), (2.2) and (2.3), rewriting the total fields \mathbf{E} and \mathbf{H} as the sum of known fields and some unknown *secondary fields* [4]. We define the secondary fields

$$\sigma' := \sigma - \sigma_0, \quad (2.5a)$$

$$\mathbf{E}' := \mathbf{E} - \mathbf{E}_0, \quad (2.5b)$$

$$\mathbf{H}' := \mathbf{H} - \mathbf{H}_0, \quad (2.5c)$$

where σ_0 is a reference conductivity, and \mathbf{E}_0 and \mathbf{H}_0 are known electric and magnetic fields induced by the sources in the reference conductivity. The fields \mathbf{E}_0 and \mathbf{H}_0 satisfy

$$\nabla \times \mathbf{E}_0 - \iota\omega\mu\mathbf{H}_0 = \mathbf{J}_m, \quad (2.6a)$$

$$\nabla \times \mathbf{H}_0 - \sigma_0\mathbf{E}_0 = \mathbf{J}_e, \quad (2.6b)$$

as well as the original boundary conditions (2.3), so

$$\mathbf{E}_0|_{\partial\Omega} = \mathbf{g}_1|_{\partial\Omega}, \quad (2.7a)$$

$$\mathbf{H}_0|_{\partial\Omega} = \mathbf{g}_2|_{\partial\Omega}. \quad (2.7b)$$

Substituting the definitions (2.5) for \mathbf{E}_0 and \mathbf{H}_0 into the original system (2.2)-(2.4), and using the half-space relations (2.6), we get the system

$$\nabla \times \mathbf{E}' - \imath\omega\mu\mathbf{H}' = \mathbf{0}, \quad (2.8a)$$

$$\nabla \times \mathbf{H}' - \sigma\mathbf{E}' = (\imath\omega\mu)^{-1}\mathbf{s}_E, \quad (2.8b)$$

$$\nabla \cdot \mathbf{E}' = \frac{\rho'_f}{\epsilon}, \quad (2.8c)$$

$$\nabla \cdot \mathbf{H}' = 0, \quad (2.8d)$$

$$\mathbf{E}'|_{\partial\Omega} = \mathbf{0}, \quad (2.8e)$$

$$\mathbf{H}'|_{\partial\Omega} = \mathbf{0}, \quad (2.8f)$$

where

$$\mathbf{s}_E := (\imath\omega\mu)(\sigma - \sigma_0)\mathbf{E}_0 \quad \text{and} \quad (2.8g)$$

$$\rho'_f := \rho_f - \epsilon\nabla \cdot \mathbf{E}_0. \quad (2.8h)$$

Since the obtained system (2.8) involves only the secondary fields \mathbf{E}' and \mathbf{H}' , we drop the primes in the sequel and use \mathbf{E} and \mathbf{H} to represent the secondary fields.

2.3 Reduction to a second-order system

To eliminate \mathbf{H} from the system (2.8), take the curl of (2.8a) and use this result to eliminate $\nabla \times \mathbf{H}$ in (2.8b), obtaining the system

$$\nabla \times \nabla \times \mathbf{E} - \imath\omega\mu\sigma\mathbf{E} = \mathbf{s}_E \quad (2.9a)$$

$$\mathbf{E}|_{\partial\Omega} = \mathbf{0} \quad (2.9b)$$

which involves only \mathbf{E} (see, e.g., [17, 16]). Once we have \mathbf{E} we get also \mathbf{H} from (2.8a). Notice that the problem (2.9) is well-posed only if $\imath\omega\mu\sigma \neq 0$. Specifically, in the limit as $|\imath\omega\mu\sigma| \rightarrow 0$, the system (2.9a) tends towards the singular system $\nabla \times \nabla \times \mathbf{E} = \mathbf{s}_E$. Thus, in solving (2.9), we cannot take advantage of the smoothing properties of elliptic operators since the system is not strongly elliptic [6, 2]. This system is also inconvenient due to the strong coupling of the different components of \mathbf{E} in the leading-order terms.

Given that the continuous problem (2.9) is singular where $\sigma \equiv 0$, practitioners often introduce a small, artificial conductivity in the air, say $\sigma \simeq 10^{-6}$, to eliminate the singular behaviour [17, 16, 24]. This regularizes the forward

modelling problem. However, any numerical scheme which faithfully models the continuous problem (2.9) produces an ill-conditioned linear system, even with $0 < \sigma \ll 1$ in the air. It is the near-singular behaviour of the underlying continuous problem that accounts for the ill-conditioned linear systems in experiments such as reported in [17]. The small conductivity term can regularize a large second-order differential term effectively only if it is added to the null space of the differential term; this does not happen in (2.9a).

2.4 Decomposition of the electric field

We want to find a continuous formulation that leads to a robust numerical discretization. We use a Helmholtz decomposition as in [3, 8, 15] and separate the electric field \mathbf{E} into two parts. The first part lies in the *active* space of the **curl** operator and the second part lies in the *null* space of the **curl** operator. That is,

$$\mathbf{E} = \mathbf{A} + \nabla\phi, \quad (2.10)$$

for some vector field \mathbf{A} and scalar field ϕ . Since $\nabla \times \nabla\phi = 0$, the field $\nabla\phi$ lies in the null space of the **curl** operator. The three unknown scalar fields $E^{(1)}, E^{(2)}, E^{(3)}$ have been replaced with four unknown scalar fields $A^{(1)}, A^{(2)}, A^{(3)}$, and ϕ (where $E^{(\ell)}$ and $A^{(\ell)}$ are the ℓ th components of the vector fields \mathbf{E} and \mathbf{A} respectively ($\ell \in \{1, 2, 3\}$)); therefore, we have one degree of freedom in determining \mathbf{A} and ϕ . Our particular choice is the *Coulomb gauge condition*

$$\nabla \cdot \mathbf{A} = 0. \quad (2.11)$$

The gauge condition (2.11) ensures that \mathbf{A} spans the active space of the **curl** operator.

It is useful to have a physical understanding of what \mathbf{A} and ϕ represent. Electric fields are induced by charges or by time-varying magnetic fluxes. An electric field caused by charges is the gradient of a scalar function; hence, $\nabla\phi$ represents the electric field due to charge accumulation. The remaining term \mathbf{A} is the electric field induced by magnetic fluxes. No charge is associated with the term \mathbf{A} , so, $\nabla \cdot \mathbf{A} = 0$. Further, from (2.8a) and (2.10),

$$\nabla \times \mathbf{A} = \nabla \times \mathbf{E} = \omega\mu\mathbf{H},$$

so $(i\omega\mu)^{-1}\mathbf{A}$ is the vector potential field for the magnetic field \mathbf{H} . The two parts of \mathbf{E} therefore correspond to the potential fields produced by distinct types of sources.

Substituting the decomposition (2.10) and the gauge condition (2.11) into the system (2.9a), we find

$$\begin{aligned}\nabla \times \nabla \times \mathbf{E} - i\omega\mu\sigma\mathbf{E} &= \nabla \times \nabla \times (\mathbf{A} + \nabla\phi) - i\omega\mu\sigma(\mathbf{A} + \nabla\phi) \\ &= \nabla \times \nabla \times \mathbf{A} - i\omega\mu\sigma(\mathbf{A} + \nabla\phi) \\ &= (-\nabla^2\mathbf{A} + \nabla(\nabla \cdot \mathbf{A})) - i\omega\mu\sigma(\mathbf{A} + \nabla\phi) \\ &= -\nabla^2\mathbf{A} - i\omega\mu\sigma(\mathbf{A} + \nabla\phi).\end{aligned}$$

Thus, we have a system of four PDEs in the four scalar unknowns $A^{(1)}$, $A^{(2)}$, $A^{(3)}$, and ϕ . The new system is

$$\nabla^2\mathbf{A} + i\omega\mu\sigma(\mathbf{A} + \nabla\phi) = -\mathbf{s}_E \quad (2.12a)$$

$$\nabla \cdot \mathbf{A} = 0. \quad (2.12b)$$

We prefer (2.12a) to (2.9a) because, for $|i\omega\mu\sigma| = O(1)$, the dominant term in the left-hand side is the term $\nabla^2\mathbf{A}$, even in the limit of low conductivities. We can exploit this strong ellipticity of the differential operator in the construction of good numerical schemes [5, 6].

There are two options to continue. One is to solve the system (2.12) directly. This system resembles the Stokes problem that describes the flow of a viscous, incompressible fluid [5, 7]. There, \mathbf{A} corresponds to the velocity field, ϕ corresponds to the pressure, and (2.12b) corresponds to the incompressibility assumption. However, a careful discretization of the system (2.12) requires a staggered grid or a marker-and-cell method (see, e.g., [5, 9]) that is difficult to implement. Moreover, while the three scalar equations in (2.12a) have $A^{(\ell)}$ ($\ell \in \{1, 2, 3\}$) in their respective dominant terms, the fourth equation (2.12b) does not involve ϕ directly. Since the PDEs (2.12) are strongly coupled and none of these equations have dominant differential terms involving ϕ in the left-hand side, construction of robust numerical solution methods for the system (2.12) requires special care.

We opt for the second approach by taking the divergence of equation (2.12a) as in [8], and simplifying using the Coulomb gauge (2.11), obtaining

$$\nabla \cdot (\sigma\nabla\phi) + \nabla \cdot (\sigma\mathbf{A}) = -(i\omega\mu)^{-1}\nabla \cdot \mathbf{s}_E. \quad (2.13)$$

A system analogous to (2.12a) and (2.13) has been studied in the context of the Navier-Stokes' equations in [12, 19, 11]. In that setting, the equation resembling (2.13) is called the *pressure-Poisson equation* since the Poisson-like term $\nabla \cdot (\sigma \nabla \phi)$ is the dominant term in the left-hand side. The new PDE system (2.12a) and (2.13) is diagonally dominant, because each of the unknown scalar fields occurs in the leading term of one of the scalar equations. Thus, the system is weakly coupled. Below, we devise numerical schemes that naturally take advantage of this structure. Further, the unknowns can be discretized without staggered grids; this makes implementation much easier.

The “pressure-Poisson” equation (2.13) is not defined in the air (because $\sigma \equiv 0$ in Ω_2), so the system (2.12a)-(2.13) is still singular in the air. However, if we don't solve for ϕ in Ω_2 , we have enough information. That is, given appropriate boundary conditions, the system has a unique solution with \mathbf{A} defined throughout Ω and ϕ defined only throughout $\Omega_1 \cup \Gamma$. Ignoring ϕ in Ω_2 corresponds to ignoring the part of the solution that lies in the null space of the original operator in (2.8).

If, for some reason, we need to know ϕ in Ω_2 , then we need more information to obtain a nonsingular system in the air. Using the divergence condition (2.8c) for \mathbf{E} ,

$$\frac{\rho_f}{\epsilon} = \nabla \cdot \mathbf{E} = \nabla \cdot (\mathbf{A} + \nabla \phi) = 0 + \nabla^2 \phi,$$

since $\nabla \cdot \mathbf{A} = 0$. We do not know the free charge density ρ_f in the ground Ω_1 ; however, since $\nabla \phi$ is the electric field caused by charges it is reasonable to assume that $\rho_f \equiv 0$ in Ω_2 (i.e., there are no free charges in the air). This additional information allows determination of ϕ in Ω_2 . Thus, the PDE system determining \mathbf{A} and ϕ throughout Ω is

$$\nabla^2 \mathbf{A} + i\omega\mu\sigma(\mathbf{A} + \nabla \phi) = -\mathbf{s}_E, \quad (x, y, z) \in \Omega_1, \quad (2.14a)$$

$$\nabla \cdot (\sigma \mathbf{A}) + \nabla \cdot (\sigma \nabla \phi) = -(i\omega\mu)^{-1} \nabla \cdot \mathbf{s}_E, \quad (x, y, z) \in \Omega_1, \quad (2.14b)$$

$$\nabla^2 \mathbf{A} = -\mathbf{s}_E, \quad (x, y, z) \in \Omega_2, \quad (2.14c)$$

together with

$$\nabla^2 \phi = 0, \quad (x, y, z) \in \Omega_2. \quad (2.14d)$$

Although it is possible to solve for ϕ in the air, in most applications it is not needed. We therefore ignore (2.14d) and restrict our attention to equations

(2.14) which determine \mathbf{A} throughout Ω and ϕ in Ω_1 given suitable boundary conditions.

2.5 Boundary conditions

Studying (2.14) requires boundary conditions for \mathbf{A} and ϕ . Recall that the scalar field ϕ is the (secondary) electric field due to charge accumulation. For controlled source experiments, the electric fields approach zero at sufficiently large distances from the sources, so we assume that there is no charge accumulation near infinity.

This yields homogeneous Dirichlet or Neumann boundary conditions. For instance, we choose

$$\phi|_{\partial\Omega_1} = 0 \quad (2.15a)$$

$$\mathbf{A}|_{\partial\Omega} = \mathbf{0}. \quad (2.15b)$$

Thus, the determination of the additional boundary condition needed for (2.13) (which is a major issue in the Navier-Stokes context [11, 19]) is resolved here in a simple way.

The field \mathbf{A} is continuous across the interface Γ , so there is no boundary condition required to determine $\mathbf{A}|_{\Gamma}$. However, to find $\phi|_{\Gamma}$, a boundary condition is needed to connect the distinct equations (2.14b) and (2.14d) determining ϕ throughout Ω . Recall that no electric current flows across the air-ground interface. This is expressed as

$$\sigma(\mathbf{A} + \nabla\phi) \cdot \mathbf{n}|_{\Gamma} = 0. \quad (2.15c)$$

The Neumann condition (2.15c) at the air-earth interface is used to determine the values of $\phi|_{\Gamma}$.

In the next section, we use a vertex-based finite-volume approach (see, e.g., [25, 19]) to discretize the equations (2.14) subject to the boundary conditions (2.15).

3 Deriving a discretization

3.1 The discrete domain

We define a three-dimensional rectangular grid, a cross-section of which is depicted in Figure 2. The vertex numbered (i, j, k) corresponds to the point

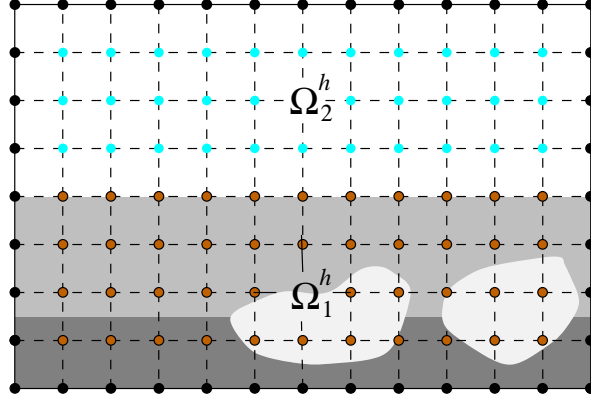


Figure 2: Discretization of the spatial domain.

with Cartesian coordinates (x_i, y_j, z_k) (where $i = 0: N_x$, $j = 0: N_y$, and $k = 0: N_z$). For convenience, define the sets

$$\begin{aligned}
\overline{\Omega}^h &:= \{(i, j, k) \mid i = 0: N_x, j = 0: N_y, k = 0: N_z\}, \\
\Omega^h &:= \{(i, j, k) \mid i = 1: N_x - 1, j = 1: N_y - 1, k = 1: N_z - 1\}, \\
\partial\Omega^h &:= \overline{\Omega}^h \setminus \Omega^h, \\
\Omega_1^h &:= \{(i, j, k) \in \Omega^h \mid k = 1: M_z - 1\}, \quad \text{and} \\
\Omega_2^h &:= \{(i, j, k) \in \Omega^h \mid k = M_z: N_z - 1\}.
\end{aligned}$$

Then, Ω^h denotes indices of vertices in the interior of the domain, Ω_1^h denotes indices of vertices in the ground portion of the domain, and Ω_2^h denotes indices of vertices in the air. Notice that the indices of vertices on the air-earth interface Γ are included in the set Ω_1^h . The remaining indices correspond to vertices on the boundary $\partial\Omega^h$.

The cells are the rectangular boxes made by joining the vertices. The cell $(i - \frac{1}{2}, j - \frac{1}{2}, k - \frac{1}{2})$ is the cell with vertices $(i - \xi, j - \eta, k - \zeta)$ (where $\xi, \eta, \zeta \in \{0, 1\}$). The lengths of the sides of this cell are

$$h_{i-\frac{1}{2}}^x := x_i - x_{i-1}, \quad h_{j-\frac{1}{2}}^y := y_j - y_{j-1}, \quad \text{and} \quad h_{k-\frac{1}{2}}^z := z_k - z_{k-1}.$$

3.2 The discrete fields

The unknown quantities are the values of \mathbf{A} and ϕ at the vertices of the grid. Specifically, the unknowns are

$$\begin{aligned} A_{i,j,k}^{(\ell)} &\simeq A^{(\ell)}(x_i, y_j, z_k), & (i, j, k) \in \Omega^h, \ell \in \{1, 2, 3\}; & \text{ and} \\ \phi_{i,j,k} &\simeq \phi(x_i, y_j, z_k), & (i, j, k) \in \Omega_1^h. \end{aligned}$$

The values of $\mathbf{A}_{i,j,k}$ and $\phi_{i,j,k}$ on the outer boundary $\partial\Omega^h$ are known in accordance with the Dirichlet boundary conditions (2.15a,b). Thus, the total number of unknowns is

$$N := 3(N_x - 1)(N_y - 1)(N_z - 1) + (N_x - 1)(N_y - 1)(M_z - 1).$$

The conductivity σ is taken to be piecewise constant. That is, throughout the cell $(i - \frac{1}{2}, j - \frac{1}{2}, k - \frac{1}{2})$, the value of the conductivity is $\sigma_{i-\frac{1}{2}, j-\frac{1}{2}, k-\frac{1}{2}}$ ($i = 1 : N_x, j = 1 : N_y, k = 1 : M_z$). For cells in the air (ie. $k + \frac{1}{2} > M_z$), the conductivity vanishes.

3.3 The finite-volume discretization

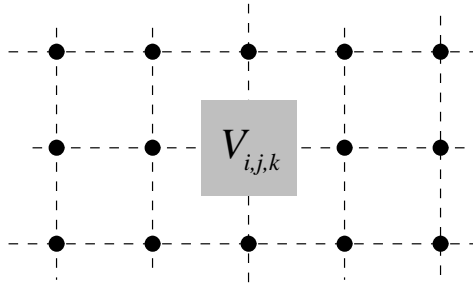


Figure 3: Cross-section of the finite volume $V_{i,j,k}$ around the vertex (i, j, k)

Consider the boxes

$$\begin{aligned} V_{i,j,k} &:= \left[x_i - \frac{h_x^{i-\frac{1}{2}}}{2}, x_i + \frac{h_x^{i+\frac{1}{2}}}{2} \right] \times \left[y_j - \frac{h_y^{j-\frac{1}{2}}}{2}, y_j + \frac{h_y^{j+\frac{1}{2}}}{2} \right] \\ &\quad \times \left[z_k - \frac{h_z^{k-\frac{1}{2}}}{2}, z_k + \frac{h_z^{k+\frac{1}{2}}}{2} \right] \end{aligned}$$

around the vertices $(i, j, k) \in \Omega^h$ as shown in Figure 3. We integrate the equations (2.14a,b) over each $V_{i,j,k}$ in the ground (ie. over all $(i, j, k) \in \Omega_1^h$) and we integrate (2.14c) over $V_{i,j,k}$ in the air (ie. over all $(i, j, k) \in \Omega_2^h$). If we need to know the potential ϕ in the air, we integrate Laplace's equation (2.14d) over the boxes $V_{i,j,k}$ in Ω_2^h as well. The resulting integrals are

$$\iiint_{V_{i,j,k}} (\nabla^2 \mathbf{A} + \imath\omega\mu\sigma (\mathbf{A} + \nabla\phi)) dV = \mathbf{F}_{i,j,k}, \quad (i, j, k) \in \Omega_1^h; \quad (3.16a)$$

$$\iiint_{V_{i,j,k}} \nabla \cdot (\sigma(\mathbf{A} + \nabla\phi)) dV = G_{i,j,k}, \quad (i, j, k) \in \Omega_1^h; \quad (3.16b)$$

$$\iiint_{V_{i,j,k}} \nabla^2 \mathbf{A} dV = \mathbf{F}_{i,j,k}, \quad (i, j, k) \in \Omega_2^h. \quad (3.16c)$$

In (3.16), the integrals of the known source terms are denoted by

$$\mathbf{F}_{i,j,k} := - \iiint_{V_{i,j,k}} \mathbf{s}_E dV \quad \text{and} \quad (3.17a)$$

$$G_{i,j,k} := -(\imath\omega\mu)^{-1} \iiint_{V_{i,j,k}} \nabla \cdot \mathbf{s}_E dV. \quad (3.17b)$$

The integrals $\mathbf{F}_{i,j,k}$ and $G_{i,j,k}$ can be integrated exactly, or by using quadrature. The integrals on the left-hand side of (3.16) separate into distinct terms

$$I_{i,j,k}^{(1,\ell)} + \imath\omega\mu \left(I_{i,j,k}^{(2,\ell)} + I_{i,j,k}^{(3,\ell)} \right) = F_{i,j,k}^{(\ell)}, \quad (i, j, k) \in \Omega^h, \ell \in \{1, 2, 3\}; \quad (3.18a)$$

$$J_{i,j,k}^{(1)} + J_{i,j,k}^{(2)} = G_{i,j,k}, \quad (i, j, k) \in \Omega_1^h; \quad \text{and} \quad (3.18b)$$

$$I_{i,j,k}^{(1,\ell)} = F_{i,j,k}^{(\ell)}, \quad (i, j, k) \in \Omega_2^h. \quad (3.18c)$$

In (3.18), the terms $I_{i,j,k}^{(k,\ell)}$ and $J_{i,j,k}^{(m)}$ ($k, \ell \in \{1, 2, 3\}$, $m \in \{1, 2\}$) are numerical approximations of the volume integrals over the boxes $V_{i,j,k}$ in (3.16). These approximations are linear combinations of the values of the discrete field

values $A_{i,j,k}^{(\ell)}$ and $\phi_{i,j,k}$ given by

$$\begin{aligned}
I_{i,j,k}^{(1,\ell)} &:= L_{i-\frac{1}{2},j,k} A_{i-1,j,k}^{(\ell)} + L_{i+\frac{1}{2},j,k} A_{i+1,j,k}^{(\ell)} + L_{i,j-\frac{1}{2},k} A_{i,j-1,k}^{(\ell)} + \\
&\quad L_{i,j+\frac{1}{2},k} A_{i,j+1,k}^{(\ell)} + L_{i,j,k-\frac{1}{2}} A_{i,j,k-1}^{(\ell)} + L_{i,j,k+\frac{1}{2}} A_{i,j,k+1}^{(\ell)} - \\
&\quad \sum_{\xi,\eta,\zeta=\pm\frac{1}{2}} (L_{i+\xi,j,k} + L_{i,j+\eta,k} + L_{i,j,k+\zeta}) A_{i,j,k}^{(\ell)} \\
&\simeq \iiint_{V_{i,j,k}} \nabla^2 A^{(\ell)} dV, \tag{3.19a}
\end{aligned}$$

$$I_{i,j,k}^{(2,\ell)} := S_{i,j,k} A_{i,j,k}^{(\ell)} \simeq \iiint_{V_{i,j,k}} \sigma A^{(\ell)} dV, \tag{3.19b}$$

$$\begin{aligned}
I_{i,j,k}^{(3,1)} &:= D_{i+\frac{1}{2},j,k} \phi_{i+1,j,k} - D_{i-\frac{1}{2},j,k} \phi_{i-1,j,k} + (D_{i-\frac{1}{2},j,k} - D_{i+\frac{1}{2},j,k}) \phi_{i,j,k} \\
&\simeq \iiint_{V_{i,j,k}} \sigma \frac{\partial \phi}{\partial x} dV, \tag{3.19c}
\end{aligned}$$

$$\begin{aligned}
I_{i,j,k}^{(3,2)} &:= D_{i,j+\frac{1}{2},k} \phi_{i,j+1,k} - D_{i,j-\frac{1}{2},k} \phi_{i,j-1,k} + (D_{i,j-\frac{1}{2},k} - D_{i,j+\frac{1}{2},k}) \phi_{i,j,k} \\
&\simeq \iiint_{V_{i,j,k}} \sigma \frac{\partial \phi}{\partial y} dV, \tag{3.19d}
\end{aligned}$$

$$\begin{aligned}
I_{i,j,k}^{(3,3)} &:= D_{i,j,k+\frac{1}{2}} \phi_{i,j,k+1} - D_{i,j,k-\frac{1}{2}} \phi_{i,j,k-1} + (D_{i,j,k-\frac{1}{2}} - D_{i,j,k+\frac{1}{2}}) \phi_{i,j,k}, \\
&\simeq \iiint_{V_{i,j,k}} \sigma \frac{\partial \phi}{\partial z} dV, \tag{3.19e}
\end{aligned}$$

$$\begin{aligned}
J_{i,j,k}^{(1)} &:= D_{i+\frac{1}{2},j,k} A_{i+1,j,k}^{(1)} - D_{i-\frac{1}{2},j,k} A_{i-1,j,k}^{(1)} + (D_{i+\frac{1}{2},j,k} - D_{i-\frac{1}{2},j,k}) A_{i,j,k}^{(1)} + \\
&\quad D_{i,j+\frac{1}{2},k} A_{i,j+1,k}^{(2)} - D_{i,j-\frac{1}{2},k} A_{i,j-1,k}^{(2)} + (D_{i,j+\frac{1}{2},k} - D_{i,j-\frac{1}{2},k}) A_{i,j,k}^{(2)} + \\
&\quad D_{i,j,k+\frac{1}{2}} A_{i,j,k+1}^{(3)} - D_{i,j,k-\frac{1}{2}} A_{i,j,k-1}^{(3)} + (D_{i,j,k+\frac{1}{2}} - D_{i,j,k-\frac{1}{2}}) A_{i,j,k}^{(3)} \\
&\simeq \iiint_{V_{i,j,k}} \nabla \cdot (\sigma \mathbf{A}) dV, \text{ and} \tag{3.19f}
\end{aligned}$$

$$\begin{aligned}
J_{i,j,k}^{(2)} &:= \tilde{D}_{i-\frac{1}{2},j,k} \phi_{i-1,j,k} + \tilde{D}_{i+\frac{1}{2},j,k} \phi_{i+1,j,k} + \tilde{D}_{i,j-\frac{1}{2},k} \phi_{i,j-1,k} + \\
&\quad \tilde{D}_{i,j+\frac{1}{2},k} \phi_{i,j+1,k} + \tilde{D}_{i,j,k-\frac{1}{2}} \phi_{i,j,k-1} + \tilde{D}_{i,j,k+\frac{1}{2}} \phi_{i,j,k+1} - \\
&\quad \sum_{\xi,\eta,\zeta=\pm\frac{1}{2}} \left(\tilde{D}_{i+\xi,j,k} + \tilde{D}_{i,j+\eta,k} + \tilde{D}_{i,j,k+\zeta} \right) \phi_{i,j,k} \\
&\simeq \iiint_{V_{i,j,k}} \nabla \cdot (\sigma \nabla \phi) dV. \tag{3.19g}
\end{aligned}$$

The coefficients L , S , D , and \tilde{D} of (3.19) are written explicitly in terms of the conductivity model $\sigma_{i-\frac{1}{2},j-\frac{1}{2},k-\frac{1}{2}}$ and the mesh spacings $h_{i-\frac{1}{2}}^x$, $h_{j-\frac{1}{2}}^y$, and $h_{k-\frac{1}{2}}^z$ in Appendix A.

In deriving the discretization (3.18),(3.19), we use Gauss' Law to reduce the volume integrals $J^{(m)}$ and $I^{(1,\ell)}$ ($\ell \in \{1,2,3\}$, $m \in \{1,2\}$) to surface integrals. From there, we use quadrature to express $I^{(k,\ell)}$ and $J^{(m)}$ ($k, \ell \in \{1,2,3\}$, $m \in \{1,2\}$) as linear combinations of the unknowns $A_{i,j,k}^{(\ell)}$ and $\phi_{i,j,k}$ (with coefficients given in Appendix A). The result is a system of $N \times N$ linear equations in N unknowns that approximates the problem (2.14),(2.15).

The discretization of the Neumann (or zero current) condition (2.15c) at the air-ground interface is a natural result of the finite-volume formulation. We see this when approximating (3.18b) over the vertices on the interface Γ using the formulae in Appendix A (using $\sigma = 0$ in the cells immediately above Γ). We expect this result since our finite-volume argument integrates over an infinitesimal volume, which is exactly how interface conditions are always derived [22]. Similarly, for layered earth or other discontinuous conductivity models, we do not need to explicitly enforce interface conditions when using a finite-volume formulation.¹

Thus, we have a 4×4 block matrix \mathcal{L} and a linear system $\mathcal{L}x = b$, where

$$\mathcal{L} := \begin{pmatrix} H_1 & & & L_1 \\ & H_1 & & L_2 \\ & & H_1 & L_3 \\ D_1 & D_2 & D_3 & H_2 \end{pmatrix}, \quad x := \begin{pmatrix} A^{(1)} \\ A^{(2)} \\ A^{(3)} \\ \phi \end{pmatrix}, \quad \text{and} \quad b := \begin{pmatrix} b^{(1)} \\ b^{(2)} \\ b^{(3)} \\ b^{(4)} \end{pmatrix}. \quad (3.20)$$

The column vector x consists of the unknown variables, ordered lexicographically (say) and stacked. The right-hand side vector b consists of the source integrals $\mathbf{F}_{i,j,k}$ and $G_{i,j,k}$ corrected (if necessary) by Dirichlet data from the boundary, ordered and stacked in the same manner as the unknowns.

4 Numerical solution of the discrete system

The system (2.14) involves four unknown scalar fields defined over a three-dimensional domain. The resulting discrete system (3.18) is very large and

¹However, if there are very large jumps in σ then the terms $J^{(m)}$ in (3.19f,g) lose accuracy. In such a case it is better to use the staggered grid discretization proposed in [13].

sparse, so we experiment with various Krylov space methods for its solution [18, 1]. There is some freedom in selecting the ordering of the equations and the unknowns, the method of preconditioning to maximize the rate of convergence, and the particular iterative method. We address the question of how to make these choices in our experiments.

There are two natural orderings for the problem. In the matrix \mathcal{L} of (3.20), the unknown fields are ordered separately, ie.

$$x = (A^{(1)}, A^{(2)}, A^{(3)}, \phi)^T$$

with the individual scalar unknowns ordered over the grid, say, lexicographically. Another natural ordering is vertex-based, where the unknowns are ordered according to their location in the grid. That is, we order the interior grid vertices and then go from vertex to vertex, listing the unknowns at each vertex, ie.

$$x = (A_1^{(1)}, A_1^{(2)}, A_1^{(3)}, \phi_1, \dots, A_i^{(1)}, A_i^{(2)}, A_i^{(3)}, \phi_i, \dots, A_M^{(1)}, A_M^{(2)}, A_M^{(3)}, \phi_M, \\ A_{M+1}^{(1)}, A_{M+1}^{(2)}, A_{M+1}^{(3)}, \dots, A_N^{(1)}, A_N^{(2)}, A_N^{(3)})^T,$$

where $M := (N_x - 1)(N_y - 1)(M_z - 1)$. The vertex-based ordering yields a matrix $\tilde{\mathcal{L}}$ whose bandwidth is narrower than the bandwidth of the matrix \mathcal{L} (see Figure 4). As a result, some preconditioners—in particular, ones based on incomplete LU-decomposition (ILU)—require less work to construct since the amount of fill-in in computing LU-decompositions grows with the bandwidth [1]. However, the convenient block structure of the matrix \mathcal{L} is lost when we use a vertex-based ordering.

For preconditioners, we consider ILUt (ILU with a threshold), Jacobi, and SOR preconditioning [10, 1]. In Section 5, we test these preconditioners with the matrices \mathcal{L} and $\tilde{\mathcal{L}}$ for problem instances of various sizes.

In (3.20), H_1 and H_2 are the dominant blocks of \mathcal{L} ; this is not surprising since H_1 and H_2 correspond to discretizations of dominant differential terms. We infer, then, that the block-diagonal matrix

$$\hat{\mathcal{L}} = \begin{pmatrix} H_1 & & & \\ & H_1 & & \\ & & H_1 & \\ & & & H_2 \end{pmatrix}$$

approximates \mathcal{L} to leading order. Thus, we construct a preconditioner that capitalizes on the block-diagonal dominance by applying ILUt to the blocks

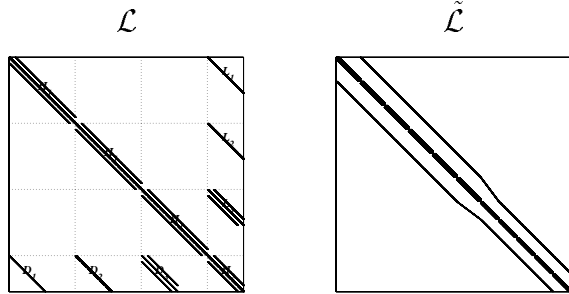


Figure 4: Sparsity patterns using lexicographic (\mathcal{L}) and vertex-based ($\tilde{\mathcal{L}}$) orderings for a system based on a $13 \times 13 \times 13$ grid. The matrix $\tilde{\mathcal{L}}$ has a much smaller bandwidth than the matrix \mathcal{L} .

H_1 and H_2 only. The result is an approximate inverse for $\hat{\mathcal{L}}$ which is an approximate inverse for \mathcal{L} in turn. Computing the approximate inverse of $\hat{\mathcal{L}}$ requires much less work and storage than applying ILU to the whole matrix \mathcal{L} . The resulting block preconditioner is

$$\begin{pmatrix} L_{H_1} & & & \\ & L_{H_1} & & \\ & & L_{H_1} & \\ & & & L_{H_2} \end{pmatrix} \begin{pmatrix} U_{H_1} & & & \\ & U_{H_1} & & \\ & & U_{H_1} & \\ & & & U_{H_2} \end{pmatrix}. \quad (4.21)$$

We denote this block preconditioner ILUBt (ILU for blocks with a threshold). In our experiments in the next section, the threshold for ILU and ILUBt is 10^{-3} .

5 Numerical Experiments and Results

5.1 A synthetic problem

To verify the accuracy of the discretization, we choose a smooth conductivity profile σ and smooth fields for \mathbf{A} and ϕ from which we construct the source field \mathbf{s}_E . The domain is $\Omega := (0, 2\pi)^3$, $\Omega_1 := (0, 2\pi) \times (0, 2\pi) \times (0, \pi)$, and

$\Omega_2 := (0, 2\pi) \times (0, 2\pi) \times (\pi, 2\pi)$. The conductivity model is

$$\sigma(x, y, z) := \begin{cases} (x+1)(y+2)(z-\pi)^2, & (x, y, z) \in \Omega_1 \\ 0, & (x, y, z) \in \Omega_2 \cup \Gamma \end{cases}.$$

We choose $\omega := 10^6 \text{Hz}$, and define \mathbf{A} and ϕ by

$$\begin{aligned} A^{(1)}(x, y, z) &:= -\sin(x) \cos(y) \cos(z), \\ A^{(2)}(x, y, z) &:= -\cos(x) \sin(y) \cos(z), \\ A^{(3)}(x, y, z) &:= 2 \cos(x) \cos(y) \sin(z), \\ \phi(x, y, z) &:= \cos(x) \cos(y) \cos(z). \end{aligned}$$

Notice $\nabla \cdot \mathbf{A} = 0$. This problem admits an exact solution while having conductivity values varying over a broad range. We generate the systems (3.20) for this synthetic problem on uniform $K \times K \times K$ grids for several integers $K > 0$. For each grid, we obtain the numerical solution x by solving the linear system of equations and compare x to the analytic solution \tilde{x} .

We use BICGSTAB with an ILU_t preconditioner to solve the problem (3.20) for x . To verify that the method is working, we compute the error, the relative residual, and the divergence of the computed solution. The results of the synthetic runs are summarized in Table 1.

K	$\ \tilde{x} - x\ /\sqrt{N}$	$\ \mathcal{L}\tilde{x} - b\ /\ b\ $	$\ \nabla \cdot \mathbf{A}\ /\sqrt{N_A}$	h^2
9	5.9×10^{-2}	1.6×10^{-1}	1.4×10^{-1}	4.8×10^{-1}
17	2.7×10^{-2}	6.6×10^{-2}	6.8×10^{-2}	1.3×10^{-1}
25	1.5×10^{-2}	3.7×10^{-2}	4.2×10^{-2}	6.3×10^{-2}
33	1.0×10^{-2}	2.4×10^{-2}	3.0×10^{-2}	3.4×10^{-2}
51	5.7×10^{-3}	1.2×10^{-2}	2.0×10^{-2}	1.6×10^{-2}

Table 1: Solution of the synthetic problem on various grids. Above, $N := (N_x - 1)(N_y - 1)(3(N_z - 1) + M_z - 1)$ is the total number of unknowns, $N_A := 3(N_x - 1)(N_y - 1)(N_z - 1)$ is the number of unknowns $A_{i,j,k}^{(1)}$, $A_{i,j,k}^{(2)}$, $A_{i,j,k}^{(3)}$, and h is the mesh size. We use the standard Euclidean 2-norm.

The second column of Table 1 implies that the computed solution of the discrete linear system is an accurate approximation of the analytic solution. The discretization seems second-order accurate as expected. Moreover, even

though the gauge condition (2.11) is not explicitly enforced, the computed solution does satisfy it to within the level of truncation error.

Next, we solve the synthetic problem repeatedly on a $25 \times 25 \times 25$ grid (the corresponding system having 55000 unknowns). We compare the efficacy of the Krylov space methods BICGSTAB, GMRES(5) and QMR (preconditioned using each of the preconditioners discussed in Section 4), recording the number of iterations and the amount of work (measured in gigaflops) to achieve convergence in each trial. For convergence, we require that the relative residual norm shrinks below 10^{-5} within 500 iterations; otherwise, the result of the trial is “*NC*” (non-convergent). In the case of ILU preconditioning, the gigaflop count includes the work to construct the preconditioning matrices in addition to the work for the iterations. The results are summarized in Table 2.

Method	Preconditioner	Iterations		Gigaflops	
		\mathcal{L}	$\tilde{\mathcal{L}}$	\mathcal{L}	$\tilde{\mathcal{L}}$
GMRES(5)	Jacobi	498	498	30	30
	SOR	423	369	11	9.2
	ILUt(10^{-3})	135	131	67	31
	ILUBt(10^{-3})	156		8.4	
BICGSTAB	Jacobi	188	188	5.4	5.4
	SOR	158	144	5.5	5.4
	ILUt(10^{-3})	21	16	22	26
	ILUBt(10^{-3})	29		3.4	
QMR	Jacobi	<i>NC</i>	<i>NC</i>	<i>NC</i>	<i>NC</i>
	SOR	<i>NC</i>	456	<i>NC</i>	31
	ILUt(10^{-3})	233	201	79	48
	ILUBt(10^{-3})	278		10	

Table 2: Comparison of performance of various preconditioned Krylov space methods on the synthetic problem.

According to Table 2, the most efficient solver for the system is BICGSTAB. In general, all of the preconditioners work fairly well with each Krylov space method except ILUt which requires the most work in each case. As expected, ILUt requires less work when applied to $\tilde{\mathcal{L}}$ as opposed to \mathcal{L} . However, ILUt does not perform particularly well regardless of the ordering. In terms

of flop counts, SOR and ILUBt are the leading preconditioners. QMR and GMRES(5) are either slow to converge or nonconvergent. Thus, from our experiments, we identify BICGSTAB as a good iterative method and ILUBt as a good preconditioner for constructing a robust solver for the forward modelling problem.

As a final check, we compare solving (2.14),(2.15) for the fields \mathbf{A} and ϕ to solving (2.9) for the field \mathbf{E} . The fields are almost exactly as determined in our synthetic problem except that we set $\sigma = 10^{-9}$ S/m in the air to regularize (2.9). We use our method to discretize (2.14),(2.15) on a uniform $25 \times 25 \times 25$ grid and we use the conservative discretization of [17, 16] for (2.9) on the corresponding staggered grid. For consistency with [17, 16] we use a Jacobi preconditioning, although for our (\mathbf{A}, ϕ) -formulation there are better preconditioners as Table 2 clearly indicates. We then apply GMRES(5) and BICGSTAB with a convergence criterion of 10^{-6} to obtain solutions for the resulting discrete systems. Our findings are summarized in Table 3.

Method	Iterations		Gigaflops	
	(\mathbf{A}, ϕ)	\mathbf{E}	(\mathbf{A}, ϕ)	\mathbf{E}
GMRES(5)	1490	3170	18.6	31.6
BICGSTAB	250	597	4.3	8.1

Table 3: Solving the synthetic problem with the (\mathbf{A}, ϕ) -formulation versus the \mathbf{E} -formulation.

The results of Table 3 demonstrate the advantage of the method using the (\mathbf{A}, ϕ) -formulation. Note that the two formulations require about the same work per iteration. This may look surprising given that the (\mathbf{A}, ϕ) -formulation involves a larger system with more unknowns; however, the number of nonzero entries in the matrix for the (\mathbf{A}, ϕ) -formulation (512350 nonzeros in a 55000^2 matrix) is close to the corresponding number for the \mathbf{E} -formulation (475824 nonzeros in a 38088^2 matrix). This stems from the strong coupling between the components in the higher-order terms of (2.9a) as compared to the weak coupling of the components of \mathbf{A} and ϕ in (2.14). We emphasize that, although these comparisons are based on a synthetic problem, the trends observed in Table 3 are general.

5.2 A geophysical test problem

To test our algorithm, we compute the electric field at the surface of the earth due to an incident plane wave. This is the basic computation required in a magnetotelluric (MT) experiment [16]. The frequency used is $\omega = 10^3$ Hz. The conductivity profile is a block of high conductivity (10 S/m) in a low conductivity background (0.01 S/m). The goal is to find the electric field at the surface of the earth Γ for the given frequency. The conductivity model is plotted in Figure 5.

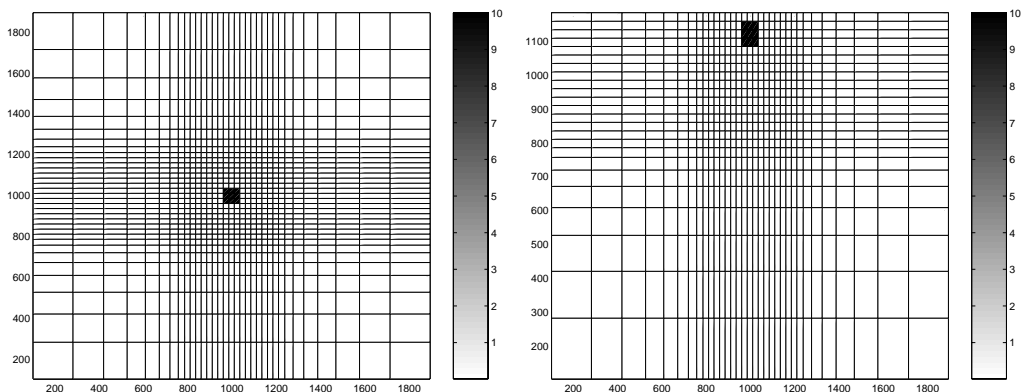


Figure 5: Cross-sections of the conductivity model.

To approximate the boundary conditions at infinity, we generate a finite but exponentially increasing grid on which we solve the problem. Starting with a rectangular domain with a uniform grid at the center (the cells of this uniform grid being one tenth of a skin depth in width), we pad the outside of the central grid with a layer of cells of width 1.3 times wider than the layer inside it. We keep adding layers of cells, stretching the widths at the same local grid ratio of $r = 1.3$, until the grid encompasses $l = 3$ skin depths in each direction.

We solve the MT problem using this exponentially increasing grid (shown in Figure 5). Our solution is presented in Figure 6. We solve this problem using BICGSTAB with the ILUBt preconditioner; the solution is obtained in 24 iterations. We observe from solving the problem on a large domain with various nonuniform grids that the number of iterations does not change significantly as long as $\omega\mu\sigma h \ll 1$, where h is the maximum grid spacing.

This condition essentially ensures that the dominant differential terms in (2.14) remain dominant after discretization.

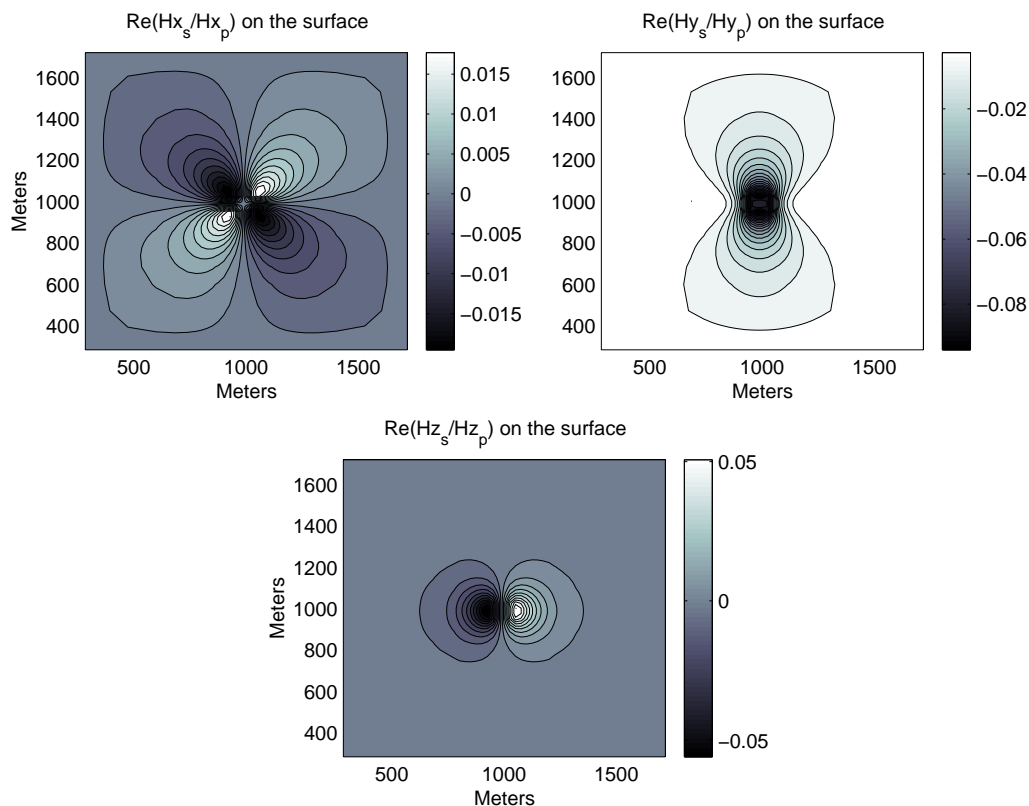


Figure 6: Solution of the MT problem. Above, \mathbf{H}_p is the primary magnetic field and \mathbf{H}_s is the secondary magnetic field. The values are taken on the air-earth interface Γ .

This MT problem obviously does not admit a closed form solution. To verify our solution, we compute the solution again using another code [16]². That code uses the \mathbf{E} -formulation (2.9), so we have to numerically differentiate ϕ from our solution to compare results. The results of both runs are similar to within discretization errors and the discrepancies are less than 5%. Thus, having first verified the accuracy and robustness of our discretiza-

²available from <http://www.cg.emr.ca/mtnet>.

tion on a toy problem, we now have confidence that our method can also be applied to physical problems.

Appendix A: Details of the discretization

The coefficients L , S , D and \tilde{D} of (3.19) are

$$\begin{aligned}
L_{i-\frac{1}{2},j,k} &:= \frac{1}{4h_{i-\frac{1}{2}}^x} \sum_{\eta,\zeta=\pm\frac{1}{2}} h_{j+\eta}^y h_{k+\zeta}^z, \\
L_{i,j-\frac{1}{2},k} &:= \frac{1}{4h_{j-\frac{1}{2}}^y} \sum_{\xi,\zeta=\pm\frac{1}{2}} h_{i+\xi}^x h_{k+\zeta}^z, \\
L_{i,j,k-\frac{1}{2}} &:= \frac{1}{4h_{k-\frac{1}{2}}^z} \sum_{\xi,\eta=\pm\frac{1}{2}} h_{i+\xi}^x h_{j+\eta}^y, \\
S_{i,j,k} &:= \frac{1}{8} \sum_{\xi,\eta,\zeta=\pm\frac{1}{2}} h_{i+\xi}^x h_{j+\eta}^y h_{k+\zeta}^z \sigma_{i+\xi,j+\eta,k+\zeta}, \\
D_{i-\frac{1}{2},j,k} &:= \frac{1}{2} h_{i-\frac{1}{2}}^x \tilde{D}_{i-\frac{1}{2},j,k}, \\
D_{i,j-\frac{1}{2},k} &:= \frac{1}{2} h_{j-\frac{1}{2}}^y \tilde{D}_{i,j-\frac{1}{2},k}, \\
D_{i,j,k-\frac{1}{2}} &:= \frac{1}{2} h_{k-\frac{1}{2}}^z \tilde{D}_{i,j,k-\frac{1}{2}}, \\
\tilde{D}_{i-\frac{1}{2},j,k} &:= \frac{1}{4h_{i-\frac{1}{2}}^x} \sum_{\eta,\zeta=\pm\frac{1}{2}} h_{j+\eta}^y h_{k+\zeta}^z \sigma_{i-\frac{1}{2},j+\eta,k+\zeta}, \\
\tilde{D}_{i,j-\frac{1}{2},k} &:= \frac{1}{4h_{j-\frac{1}{2}}^y} \sum_{\xi,\zeta=\pm\frac{1}{2}} h_{i+\xi}^x h_{k+\zeta}^z \sigma_{i+\xi,j-\frac{1}{2},k+\zeta}, \\
\tilde{D}_{i,j,k-\frac{1}{2}} &:= \frac{1}{4h_{k-\frac{1}{2}}^z} \sum_{\xi,\eta=\pm\frac{1}{2}} h_{i+\xi}^x h_{j+\eta}^y \sigma_{i+\xi,j+\eta,k-\frac{1}{2}}.
\end{aligned}$$

References

- [1] R. Barrett, M. Berry, T.F. Chan, J. Demmeland, J. Donato, J. Donarra, V. Eijkhout, R. Pozo, C. Romine, and H. Van der Vorst. *Tem-*

- plates for the Solution of Linear Systems: Building Blocks for Iterative Methods.* SIAM, Philadelphia, 1994.
- [2] G. Birkhoff and R.E. Lynch. *Numerical Solution of Elliptic problems.* SIAM, 1984.
 - [3] O. Bíró and K. Preis. On the use of the magnetic vector potential in the finite element analysis of three-dimensional eddy currents. *IEEE Transactions on Magnetics*, 25:3145–3159, 1989.
 - [4] M. Born. *Principles of Optics.* Pergamon Press, 5th ed, 1975.
 - [5] A. Brandt. Multigrid techniques: 1984 Guide with applications to fluid Dynamics. The Weizmann Institute of Science, Rehovot, Israel, 1984.
 - [6] A. Brandt and N. Dinar. Multigrid solution to elliptic flow problems. In *Numerical Methods for PDE's*, pages 53–147. Academic Press, New York, 1979.
 - [7] C. Canuto, M.Y. Hussaini, A. Quarteroni, and T.A. Zang. *Spectral Methods in Fluid Dynamics.* Springer-Verlag, 1987.
 - [8] M.E. Everett and A. Schultz. Geomagnetic induction in a heterogenous sphere: Azimuthally symmetric test computations and the response of an undulating 660-km discontinuity. *J. Geophys. Res.*, 101:2765–2783, 1996.
 - [9] C.A.J. Fletcher. *Computational Techniques for Fluid Dynamics*, volume II. Springer-Verlag, 1988.
 - [10] G.H. Golub and C.F. Van Loan. *Matrix Computations.* Johns Hopkins University Press, 1983.
 - [11] P. M. Gresho and R. L. Sani. On pressure boundary conditions for the incompressible Navier-Stokes equations. *Internat. J. Numer. Methods Fluids*, 7:1111–1145, 1987.
 - [12] P.M. Gresho. Some current issues relevant to the incompressible navier-stokes equations. *Comput. Methods Appl. Mech. Engrg.*, 87:201–252, 1987.

- [13] E. Haber, U. Ascher, D. Aruliah, and D. Oldenburg. Fast modelling of 3D electromagnetic using potentials. Technical report, Institute of Applied Mathematics, University of British Columbia, 1999.
- [14] J.M. Hyman and M. Shashkov. Mimetic discretizations for Maxwell's equations and equations of magnetic diffusion. Technical report, Los Alamos Nat. Lab., 1998. LA-UR-98-1032.
- [15] D.J. LaBrecque. A scalar-vector potential solution for 3D EM finite-difference modeling. In M. Oristaglio and B. Spies, editors, *International Symposium on Three-Dimensional Electromagnetics*, pages 143–149. Schlumberger-Doll Research, 1995.
- [16] R.L. Mackie, T.R. Madden, and P.E. Wannamaker. Three dimensional magnetotelluric modeling using difference equations - theory and comparison to integral equation solutions. *Geophysics*, 58:215–226, 1993. vol 2.
- [17] G.A. Newman and D.L. Alumbaugh. Frequency-domain modelling of airborne electromagnetic responses using staggered finite differences. *Geophys. Prospecting*, 43:1021–1042, 1995.
- [18] Y. Saad. *Iterative Methods for Sparse Linear Systems*. PWS Publishing Company, 1996.
- [19] D. Sidilkover and U. Ascher. A multigrid solver for the steady state navier-stokes equations using the pressure-poisson formulation. *Comp. Appl. Math. (SBMAC)*, 14:21–35, 1995.
- [20] A.M. Stuart and A.R. Humphries. *Dynamical systems and numerical analysis*. Cambridge University Press, Cambridge, England, 1996.
- [21] A. Taflove. *Computational Electrodynamics: the Finite-Difference Time-Domain Method*. Artech House Publishers, 1995.
- [22] S.H. Ward and G.W. Hohmann. Electromagnetic theory for geophysical applications. *Electromagnetic Methods in Applied Geophysics*, 1:131–311, 1988. Soc. Expl. Geophys.
- [23] C. Weaver. *Mathematical Methods for Geo-Electromagnetic Induction*. John Wiley & Sons Inc, Philadelphia, 1994.

- [24] J.T. Weaver and A.K. Agarwal. Recent developments in three dimensional finite difference modelling of the magnetic field in geo-electric induction. *International Symposium on Three Dimensional Electromagnetics*, pages 131–142, 1995.
- [25] P. Wesseling. *An Introduction to Multigrid Methods*. John Wiley & Sons, Chichester, 1992.
- [26] C.T. Young, J.R. Booker, J. Stodt, H.S. Waff, and P.E. Wannamaker. Verification of five magnetotelluric systems in the mini-emslab experiment. *Geophysics*, 53:553–557, 1988.